Pushing the Limits of High Performance Dual-Layer Hollow Fiber Fabricated via I²PS Process in Dehydration of Ethanol

Yee Kang Ong and Tai-Shung Chung
Dept. of Chemical and Biomolecular Engineering, National University of Singapore,
10 Kent Ridge Crescent 4 Engineering Drive 4, Singapore 117576, Singapore

DOI 10.1002/aic.14149
Published online June 21, 2013 in Wiley Online Library (wileyonlinelibrary.com)

The immiscibility induced phase separation (I^2PS) process was introduced as a novel method to fabricate hollow fibers with exceptionally high water permeance and reasonably high water/ethanol selectivity in dehydration of ethanol by pervaporation. As a continuation of the previous work, this study discloses the mechanisms to enhance the performance of hollow fibers spun via I^2PS by elucidating the material selection at the inner-layer. Moreover, it revealed the methods to reduce mass-transport resistance by enhancing surface porosity for both inner and outer surfaces to further improve the permeation flux of the membranes. The continuous performance test demonstrates that the fibers spun from the I^2PS possess a stable dehydration performance throughout the monitored period of 300 h. A comparison with pervaporation membranes in the literatures verifies the superiority of the membranes spun via I^2PS process with the highest water permeation flux of 9.5 kg/m² h and the permeate water purity of 95.8 wt % at 80°C. © 2013 American Institute of Chemical Engineers *AIChE J*, 59: 3006–3018, 2013

Keywords: ethanol dehydration, pervaporation, dual-layer hollow fiber, membrane formation, stability

Introduction

Pervaporation has been considered as an emerging technology for separation since its debut by Kober in 1917.[1] The early works of pervaporation were carried out by several groups such as Binning and co-workers at the American Oil Co.,[2] Chiang and Perry at Monsanto Chemical Co.,[3,4] as well as Aptel, Neel and co-workers at the University of Toulouse.[5,6] Since then, pervaporation has continuously shown superior inherent capability to separate liquid mixtures such as azeotropic mixtures, solutions with a similar boiling point, thermal sensitive compounds, organic-organic mixtures as well as the removal of dilute organic species from wastewater.[7–18] However, the thriving era for pervaporation can only begin if highly permeable asymmetric membranes are developed and commercially available. Several commercial pervaporation membranes ranging from polymeric, inorganic to hybrid materials have been introduced such as Pervap® by Gesellschaft für Trenntechnik (GFT) (then Sulzer Chemtech),[19,20] Aquarius® by Membrane Technology and Research (MTR), Inc.,[12,13] NaA zeolite by Mitsui Engineering and Shipbuilding Co., Ltd.,[21] and Hybsi® by Pervatech B.V. (licensed from Energy Research Centre of the Netherlands).[22] Nevertheless, most inorganic membranes have the drawbacks of complicated fabrication and high cost, while most organic membranes may encounter weaknesses such as swelling, low permeation flux and poor separation factor. Thus, there are huge demands for higher performance pervaporation membranes.

Polymers remain as the most versatile and viable membrane material due to their ease of fabrication as well as relatively low-production costs as compared to inorganic membranes. The membrane fabricated in a hollow fiber form is reported to exhibit a higher packing density, self-supporting structure and self-containing vacuum channel if the shell feed mode is applied.[7,14,23] The art in hollow fiber spinning comprises a large number of control parameters throughout the entire chain of dope formulation, coagulation chemistry, spinneret design to the spinning parameters such as air gap and take-up speed. The complexity increases as the spinning method advances from the single-layer to the dual-layer hollow fibers. The dual-layer hollow fiber possesses the advantages of cost reduction as well as to provide a higher degree of freedom for the customization of materials and morphology in both selective and supporting layers.[24] This sophisticated spinning technique was demonstrated by Henne et al. in early 1980s to fabricate dialyzing membranes with an adsorbent layer.[25] Thereafter, the research on dual-layer hollow fibers has been extended into various fields of separation such as gas separation, nanofiltration, membrane distillation and pervaporation.[26–32]

The compatibility between the inner and outer layer dope solutions is an important criterion during the dual-layer hollow fiber spinning. Delamination between the inner and outer layer materials may occur if the compatibility is poor. This undesirable phenomenon may lead to the deterioration of membrane performance and structural failure.[24,32] Significant efforts have been done to elucidate and eliminate the

Additional Supporting Information may be found in the online version of this article.

Correspondence concerning this article should be addressed to T.-S. Chung at chencts@nus.edu.sg.

delamination phenomenon during the dual-layer hollow fiber spinning. Li et al.[24,32] concluded that the delamination phenomenon can be eliminated through the proper selection of bore fluid chemistry, inner-layer dope concentration and control of shrinkage rates in both inner and outer layers. Widjojo et al.[33] introduced the usage of an indented dual-layer spinneret to induce early convective premixing of polymer solutions in both inner and outer layers inside the spinneret prior to phase inversion. Besides, the delamination phenomenon can be overcome through post treatment processes such as heat treatment and solvent exchange.[24,33]

Despite the aforementioned advantages of dual-layer hollow fibers, the application of dual-layer hollow fiber spinning was extended to the fabrication of mixed matrix hollow fibers for gas separation and pervaporation where nanoparticle fillers were incorporated into the outer-layer dope solutions.[34–38] In addition, this spinning technique can be applied to design specific morphology and properties of hollow fibers through the manipulation of dope formulations in both inner and outer layers.[39–41] *In situ* polymer blending can also be done through coextruding polymer materials that are miscible in both inner and outer layer channels of the dual-layer spinneret. Jiang et al.[42] reported the usage of polysulfone and Matrimid® as outer and inner layer dope solutions, respectively to form an interpenetrating polymer network at the interface between the inner and outer layers. Furthermore, Kopéc et al.[43] reported on the usage of a triple orifice spinneret to fabricate a single-layer hollow fiber membrane with an inner selective skin by introducing the concept of "chemistry in a spinneret". A crosslinker was added to the bore fluid to induce simultaneous crosslinking and phase inversion during the spinning process, while a mixture of solvent and nonsolvent was flown at the outer layer to control the thickness of the inner selective layer.

The concept of fabricating multilayer composite membranes has been implemented in the membrane industry.[44–47] Ong and Chung[48] recently proposed an alternative single-step co-spinning method to produce high performance hollow fibers for dehydration of ethanol via pervaporation by means of the immiscibility induced phase separation (I^2PS) process. The I^2PS technique used the occurrence of phase separation phenomena in the immiscible blend dopes that induce the formation of a selective layer between the inner layer and outer layer. This membrane configuration has the advantage of preventing the selective layer from direct contact with the feed mixture through a shielding layer extruded as the outer layer. As a result, the swelling of the selective layer can be significantly reduced if a suitable outer layer material is chosen. However, the fabrication of hollow fibers with a thin selective layer embedded at the interface without sacrificing selectivity and permeation flux is very challenging. Therefore, this study aims to overcome this challenge and to explore the methods to enhance the performance of I^2PS hollow fibers by customizing the inner layer's materials as well as to reduce the mass-transfer resistance at both outer and inner layers. The separation performance and structural stability of the newly developed hollow fibers were investigated for the dehydration of ethanol at 65°C for 200 h followed by 80°C for 100 h. It is believed that this fundamental work may provide valuable insights for the development of next generation pervaporation membranes.

Experimental

Materials

Cellulose triacetate (CTA, CA-436-80S) was provided by Eastman Chemical Co., and used as the outer layer material since it has the inherently good chemical resistance and capability to form a relatively porous inner surface in the outer layer,[48] while three commercially available materials; namely (1) poly(ether imide) (PEI) known as Ultem® 1010 from SABIC innovative plastics, (2) polysulfone (PSf) known as Udel® from Solvay advanced polymers, and (3) copolyimide of 3,3′4,4′benzophenone tetracarboxylicdianhydride and 80% methylphenylenediamine + 20% methylenediamine known as P84® from HP Polymer GmbH were employed as the inner layer materials to provide a wide range of inner layer materials for the I^2PS spinning technology.

N—Methyl-2-pyrrolidone (NMP, analytical grade), acetone (technical grade), methanol (technical grade) and *n*-hexane (technical grade) were used as the solvents in this study. Ethanol (analytical grade) and deionized water were used to prepare the feed mixture for pervaporation studies. All the chemicals were used as received.

Polymer dope preparation and hollow fiber spinning

The polymers were vacuum-dried overnight prior to dope preparation. First, the polymer was gradually added to the NMP under a vigorous stirring condition and continuously stirred for 24 h to obtain a homogeneous solution. Table 1 tabulates the compositions of all dope solutions. Thereafter, the dope solutions were poured into ISCO syringe pumps and degassed overnight prior to hollow fiber spinning.

The dual-layer hollow fibers were fabricated via dry-jet wet-spinning by coextruding outer layer and inner layer polymer dopes as well as bore fluid through a triple-orifice spinneret. The detailed description of hollow fiber spinning setup had been described elsewhere.[23,24,26,27] Table 1 tabulates the spinning parameters. The as-spun fibers were immersed in water for 2 days to ensure complete removal of the residual solvent from the as-spun fibers. All the fibers were then solvent exchanged by immersing them in methanol for 30 min followed by *n*-hexane for another 30 min. Each solvent treatment was repeated three times. Finally, the fibers were air-dried at room temperature and stored prior to performance evaluation.

Characterizations

Scanning Electron Microscopy (SEM). The morphology of dual-layer hollow fibers was observed by using a field emission scanning electron microscope (FESEM JEOL JSM-6700LV). The samples were prepared by fracturing the fibers in liquid nitrogen and then coated with platinum using a sputtering coater (JEOL LFC-1300).

Positron Annihilation Spectroscopy (PAS). Slow beam positron annihilation spectroscopy (PAS) with the radioisotope of ^{22}Na (50 mCi) as the positron source was used to probe the depth profile of the dual-layer hollow fibers. The Doppler broadening energy spectra (DBES) were recorded using a high purity germanium detector (HPGe) at a counting rate of approximately 1100 cps with the total count of 1 million for each spectrum. The DBES spectra were characterized by R parameter as a function of positron implantation energy ranging from 0.1 keV to 10 keV and the implantation

Table 1. Spinning Conditions of Dual-Layer Hollow Fibers

Spinning Parameters	Conditions	
Outer-layer dope composition (wt%)	CTA/NMP (10/90)	
Inner-layer dope composition (wt%)	Ultem®/NMP (25/75);	PSf/NMP (25/75); P84®/NMP (25/75)
Bore fluid composition (wt%)	NMP/water (95/5)	
Outer layer dope flow rate (ml/min)	0.1-0.4	
Inner layer dope flow rate (ml/min)	1.5	
Bore fluid flow rate (ml/min)	1-1.2	
Air gap (cm)	1.5	
Take up speed (m/min)	Free fall	
Spinneret temperature (°C)	25	
External coagulant temperature (°C)	25	
External coagulant	Water	

depth for each sample can be correlated by the following equation[27,49–51]

$$Z(E_+)=\frac{40}{\rho}E_+^{1.6} \tag{1}$$

where Z is the average implantation depth in nm, ρ is the density of the polymer material in g/cm^3, and E_+ denotes the incident positron energy in keV. The R-parameter provides the information regarding the relative amount of large cavities in the range of nm to μm as the function of depth profile[27,45–47] which can be defined as the ratio of the total counts from valley regions with an energy width between 364.2 keV and 496.2 keV (due to 3γ annihilation) to the total counts from the 511 keV peak region with a width between 504.35 keV and 517.65 keV (due to 2γ annihilation).

Pervaporation studies

The feed solvent mixture was circulated in the shell side of the fiber at a flow rate of 0.5 L/min for each module with different feed temperatures. The downstream pressure was maintained less than 1 mbar throughout experiments and the system was stabilized for 2 h to ensure the steady state condition before the sample collection was carried out. The permeate samples were then collected by a cold trap immersed in liquid nitrogen at a certain time interval. Permeate samples were subsequently weighed by a digital balance to determine their fluxes, while the sample compositions were analyzed by an Agilent Technologies GC system (7890A gas chromatography) consisting of a HP-INNOWAX column packed with cross-linked poly(ethylene glycol) and a *thermal conductivity detector* (TCD). The feed concentration varied less than 1 wt % throughout the experiment. Therefore, it can be considered as constant due to the large quantity of the feed solution as compared to that of the permeate sample.

The flux (J) and separation factor (β) were defined as follows

$$J=\frac{Q}{A\times t} \tag{2}$$

$$\beta=\frac{y_i/y_j}{x_i/x_j} \tag{3}$$

where J is the flux, Q is the total weight of the permeate collected at a specific period (t), A is the effective surface area of the fibers.

The solution diffusion model has been accepted to describe the pervaporation process through dense membranes and hence, the trans-membrane permeation flux of a particular component can be written as[52]

$$J_i=\frac{P_i}{l}\left(f_{i,f}-f_{i,p}\right) \tag{4}$$

where P_i is the permeability of component i across the membrane, l is the thickness of the selective layer, $f_{i,f}$ and $f_{i,p}$ are fugacities or partial vapor pressures of component i on feed side and permeate side of the membrane, respectively. In this study, $f_{i,p}$ was assumed to be negligible since a high vacuum was applied in the permeate side of the membrane. The fugacity of component i in the feed side based on its liquid concentration can be determined by

$$f_{i,f}=x_i\gamma_i p_i^{sat} \tag{5}$$

where x_i, γ_i and p_i^{sat} are the mass fraction, activity coefficient and saturated vapor pressure of component i in the feed. Both activity coefficient and saturated vapor pressure in this study were obtained from Aspen Properties v7.1 provided by AspenTech, Inc., with the WILSON method. The selectivity (α) of the membrane was then defined as the permeance ratio of components i and j

$$\alpha_{ij}=\frac{P_i/l}{P_j/l} \tag{6}$$

Results and Discussion

Effects of inner layer materials on dual-layer hollow fibers

Morphology. The inner layer materials of as-spun hollow fibers were varied from PSf, Ultem® to P84®, while CTA was maintained as the outer layer material because it has the required chemical resistance as well as the inherent capability to create a relatively porous inner surface in the outer layer that minimizes the overall mass-transfer resistance across the outer layer.[48]

Figure 1 shows the general morphology of hollow fibers spun from various inner layer materials. Despite the solubility parameter of P84® is the closest to CTA among the three inner layer materials shown in Table 2,[18,33,42,53–55] the adhesion between the CTA outer and P84® inner layers is poor and delamination is visibly observed for the resultant fiber. The delamination occurs mainly due to a large difference in the shrinkage rate between the P84® inner layer and the CTA outer layer.[32] A similar phenomenon was reported by Widjojo et al. in the fabrication of Ultem®/P84® dual-layer hollow fibers.[33]

It is worth noting that the inner surface morphology of the outer layer is strongly correlated with the physicochemical properties of the inner-layer materials. The inner surface of the outer layer for hollow fibers spun from PSf is relatively

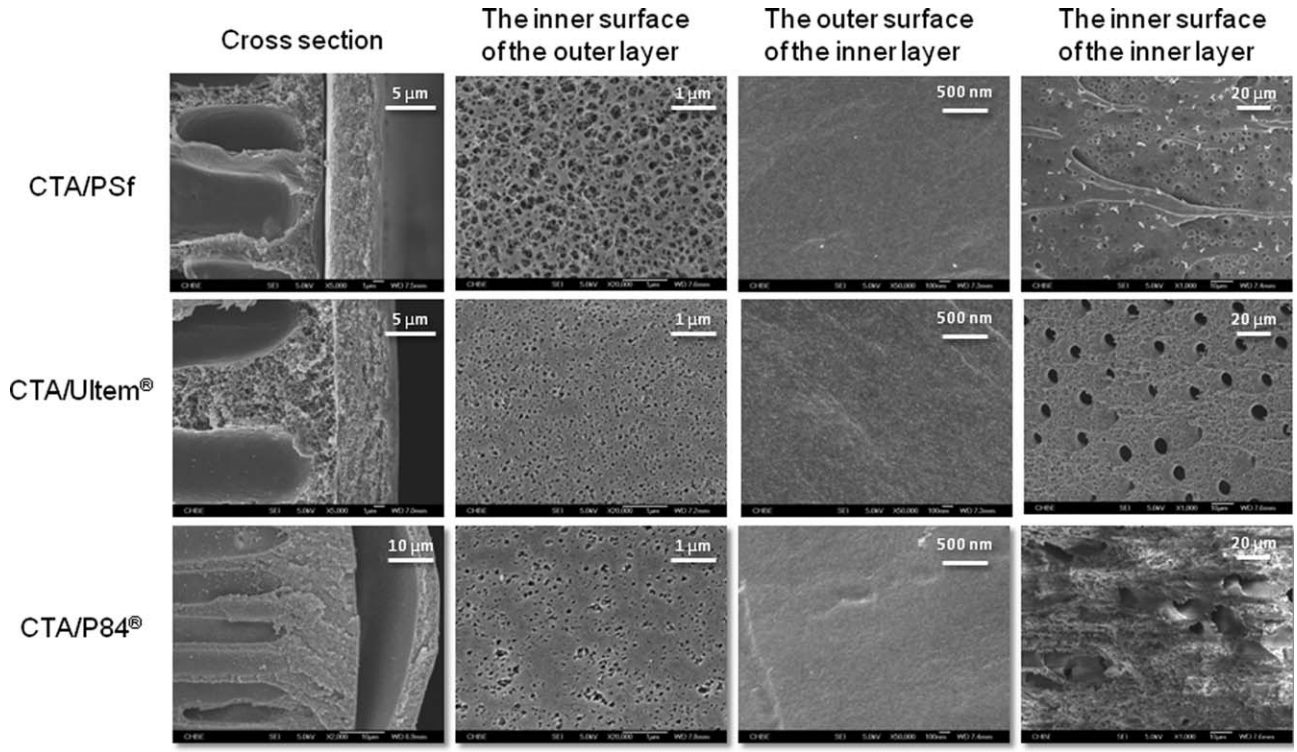

Figure 1. Morphology of the fibers spun from various inner-layer materials.

Outer-layer dope flow rate: 0.2 mL/min; inner-layer dope flow rate: 1.5 mL/min; bore fluid flow rate: 1.0 mL/min.

porous, but the porosity reduces when the inner layer material switches from PSf to Ultem® and P84®. The evolution of morphology may be elucidated from the aspects of solubility parameters of the respective polymer pairs as well as the phase inversion mechanism.

In general, solubility parameters and hydrophilicity are closely correlated. The higher the solubility parameters, the more hydrophilic the materials are. Based on the solubility parameters of the polymers in Table 2, the compatibility or miscibility of the polymer pairs are in the order of CTA-P84® > CTA-Ultem® > CTA-PSf. Therefore, a huge difference in solubility parameter between CTA and PSf may cause the rejection of both polymer dopes at the interface. It may lower the polymer concentration near the interface and induce the formation of a porous structure upon the completion of the phase inversion process. A typical example was given by Zhang et al.[49] where they reported that the hydrophilic cellulose membranes cast on a hydrophobic surface (Teflon plate) possessed more porous structure as compared to the membranes cast on a hydrophilic surface (glass plate) due to the differences in polymer-casting surface interaction. Conversely, strong interactions may occur between the outer and inner layer dope solutions of CTA and P84® due to the close solubility parameter of both polymers. The high-molecular interaction may lead to the formation of a relatively dense interfacial structure due to the faster gelation process initiated by a higher polymer concentration at the interface. Jiang et al.'s work[42] gave a typical example where polysulfone and Matrimid® formed a relatively dense layer at the interface between the inner and outer layers.

From the perspective of phase inversion, it is postulated that the hydrophobicity/hydrophilicity properties of the inner layer materials may influence the phase inversion mechanism and fiber morphology. Figure 2 portrays the phase inversion mechanisms that yield different final morphology of the as-spun fibers. The fiber spun from the PSf inner layer dope possesses relatively large macrovoids as compared to its counter parts (Ultem® and P84®). The low polymer concentration zone near the interface of PSf and CTA due to the mismatches of their solubility parameters and hydrophobicity/hydrophilicity may have created the weak points for the nonsolvent (i.e., water) intrusion. The sizes of macrovoids

Table 2. Solubility Parameters of Polymers and Solvents[18,33,42,53–55]

	Dispersion force, δ_d $(MPa)^{0.5}$	Polar force, δ_p $(MPa)^{0.5}$	Hydrogen bonding, δ_h $(MPa)^{0.5}$	Solubility Parameter, δ_{sp} $(MPa)^{0.5}$	Viscosity at room temperature (cP)
Polymers					
CTA	24.5	12.9	15.5	31.7	–
PSf	18.2	2.5	7.3	19.7	–
Ultem®	–	–	–	23.7	–
P84®	–	–	–	26.8	–
Solvents					
NMP	18.0	12.3	7.2	23.0	1.7
Ethanol	15.8	8.8	19.4	26.5	1.1
Water	15.6	16.0	42.3	47.8	0.9
Kerosene	–	–	–	15.6–15.8	1.6

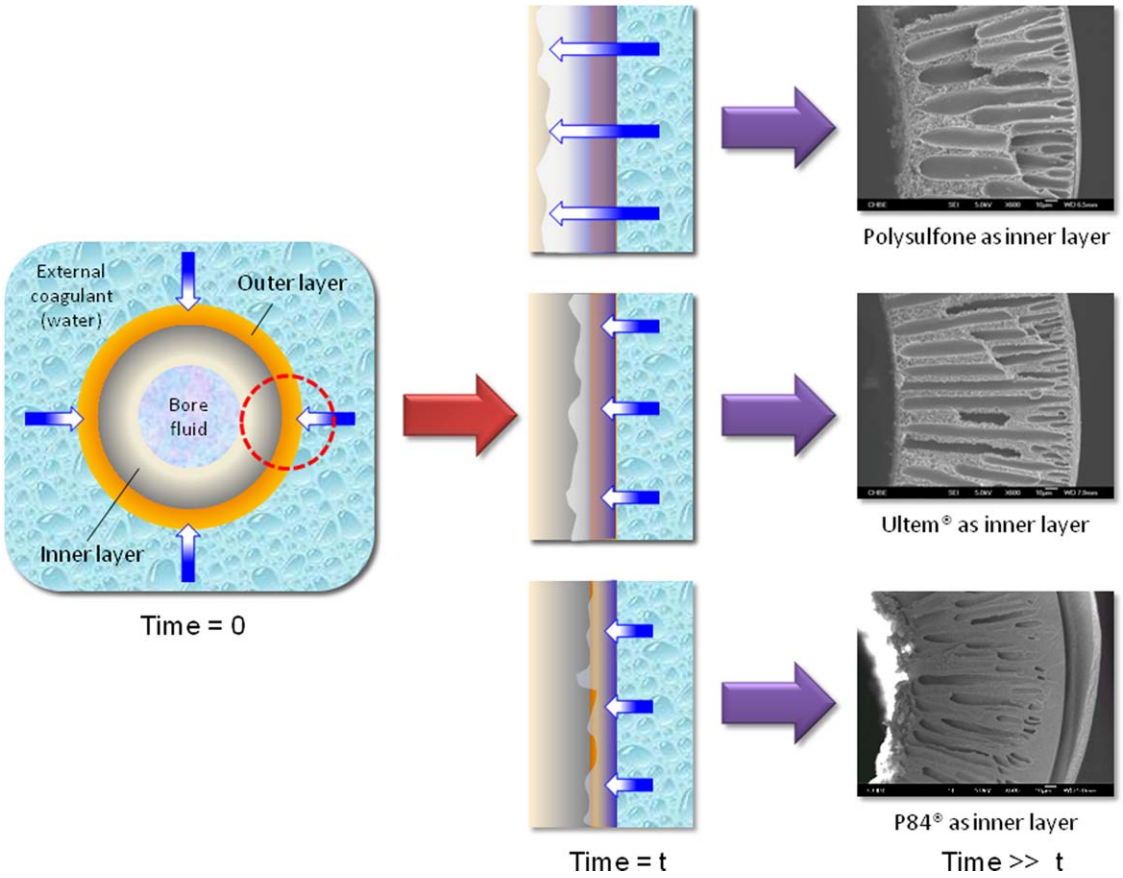

Figure 2. Proposed phase inversion mechanism for the hollow fibers spun with different inner-layer materials.

[Color figure can be viewed in the online issue, which is available at wileyonlinelibrary.com.]

become smaller when (1) the solubility parameter difference between the inner and outer layer materials is reduced, and/or (2) more hydrophilic materials such as Ultem® and P84® are applied as inner layer materials because the outer CTA layer is hydrophilic. In addition, chain entanglement plays an important role to retard the formation and propagation of macrovoids.[23] Since the critical concentration of P84® in NMP is relatively low (shown in Figure 3[33,48]), there are certain degrees of polymer chain entanglements occurring in the dope solution that may partially hinder the formation and propagation of macrovoids.[56] As a result, the fiber spun from P84® as the inner layer material possesses a sponge-like

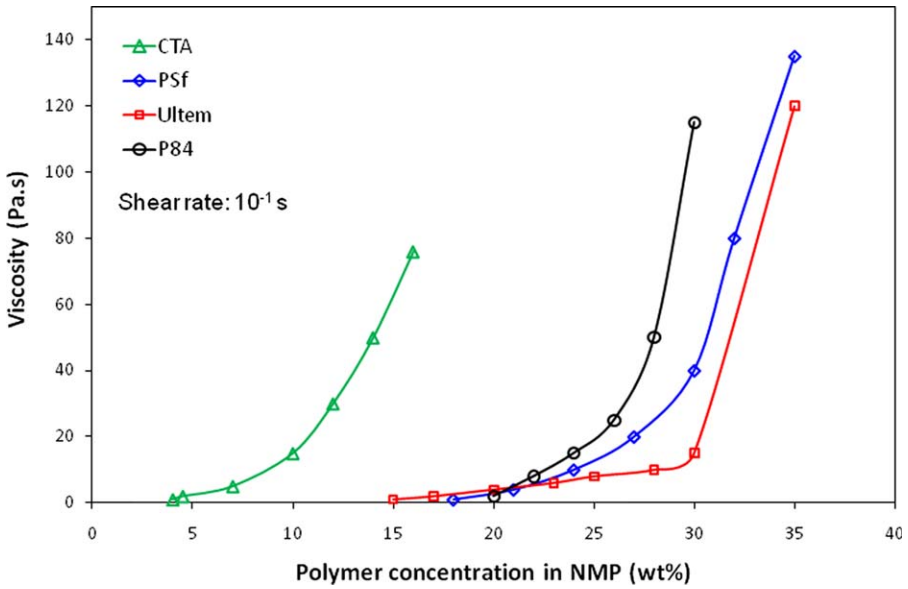

Figure 3. The shear viscosity of dope solutions as a function of polymer concentration.[33,48]

[Color figure can be viewed in the online issue, which is available at wileyonlinelibrary.com.]

Table 3. Performance of Hollow Fibers Spun from Different Inner-Layer Materials for Dehydration of Ethanol

Fiber ID	Outer-layer flow rate (ml/min)	Flux (kg/m^{2}h)	Permeate water concentration (wt %)	Separation factor (water/ethanol)
CTA/PSf	0.1	1.09	74.0	16
	0.2	0.73	76.0	18
	0.4	0.58	81.0	25
CTA/Ultem®	0.1	3.52	79.3	21
	0.2	2.81	85.2	34
	0.4	1.52	96.4	120
CTA/P84®	0.1	15.68	21.9	1.3
	0.2	12.70	24.6	1.5
	0.4	9.26	29.8	1.9
PSf	–	8.71	14.8	1
Ultem®	–	11.30	20.0	1.2
P84®	–	13.15	19.2	1.2

Inner-layer dope flow rate: 1.5ml/min; bore fluid flow rate: 1 ml/min; air gap: 1.5 cm
Feed: Ethanol/water (85/15 wt%) at 50°C

structure underneath the CTA outer layer. Similarly, since the CTA concentration is close to its critical concentration of 12 wt %[49] and its thickness is very thin,[32,57,58] the outer-layer morphology of all fibers shows a macrovoid-free structure.

Performance evaluation

The dehydration performance of hollow fibers as functions of inner layer material and outer-layer dope flow rate is tabulated in Table 3. For comparison, single-layer hollow fibers spun from exactly the same inner layer materials and dope formulations through the same triple orifice spinneret are used as the controls. All single-layer hollow fibers show insignificant separation factors, while the separation factors of all dual-layer I^{2}PS fibers increase with an increase in outer-layer flow rate. The performance enhancement is predominantly due to (1) the effectiveness of the shielding effect by the outer protective layer during the phase inversion process and (2) the reduced swelling during pervaporation experiments. In other words, a high outer-layer dope flow rate can effectively prevent the intrusion of the strong external coagulant (i.e., water) during phase inversion and thus promote the formation of a nearly defect-free selective layer at the outer-surface of the inner-layer.[48] In addition, a relatively thick CTA outer layer may restrain the swelling effect caused by the feed mixture during pervaporation experiments. However, a reduction in permeation flux is observed for fibers with a thicker CTA outer layer due to a larger mass-transfer resistance.

The data in Table 3 are replotted in terms of selectivity and permeance in Figure 4 for a direct comparison of all I^{2}PS fibers. Although P84® copolyimide has been regarded as a very robust material for pervaporation membranes,[59,60] the dual-layer hollow fibers spun from P84® co-polyimide as the inner layer material show the worst performance in terms of selectivity among all I^{2}PS fibers. This poor result arises from the occurrence of delamination between the inner layer and outer layer, thus the imperfect shielding of outer layer from intrusion may result in defects in a defective dense selective layer. In addition, the similar values in solubility parameter of both P84® and ethanol (shown in Table 2) may induce inner layer swelling and deteriorate the overall separation performance. In the case of CTA/PSf hollow fibers, they have a lower permeance but with a satisfactory selectivity. The low permeance may be attributed to the fact that, comparing with other fibers, they have relatively less porous structures in the inner layer as shown in Figure 1. As a result, they have a higher transport resistance for mass transfer. On the contrary, the fibers spun from Ultem® as the inner-layer material possess a balance in both selectivity and permeance for dehydration of ethanol. Clearly, the dehydration performance of I^{2}PS fibers is affected by the inner layer materials and CTA/Ultem® fibers are, therefore, chosen for further studies.

Reduction of mass-transfer resistance

Manipulation of the Outer Surface of the Outer Layer (i.e., Top Surface or Skin). Figure 5 portrays the top surface (i.e., the outer surface of the outer layer) morphology of the as-spun fibers obtained from the previous section, which show a relatively dense structure. These dense surfaces may provide additional mass-transfer resistance.[61] Fibers with higher permeances may be obtained if this transport resistance at the top surface is reduced. Two approaches are, therefore, explored; namely, (1) the reduction of dense layer thickness by increasing the bore fluid flow rate, and (2) the induction of a defective top surface by dual-bath spinning with the help of an acetone/water mixture as the secondary coagulant. The second approach is based on the fact that

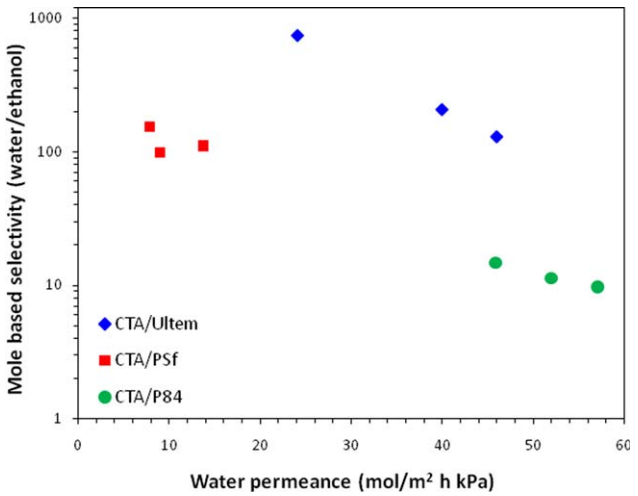

Figure 4. Graphical representations on the performance of hollow fibers as a function of inner-layer materials.

[Color figure can be viewed in the online issue, which is available at wileyonlinelibrary.com.]

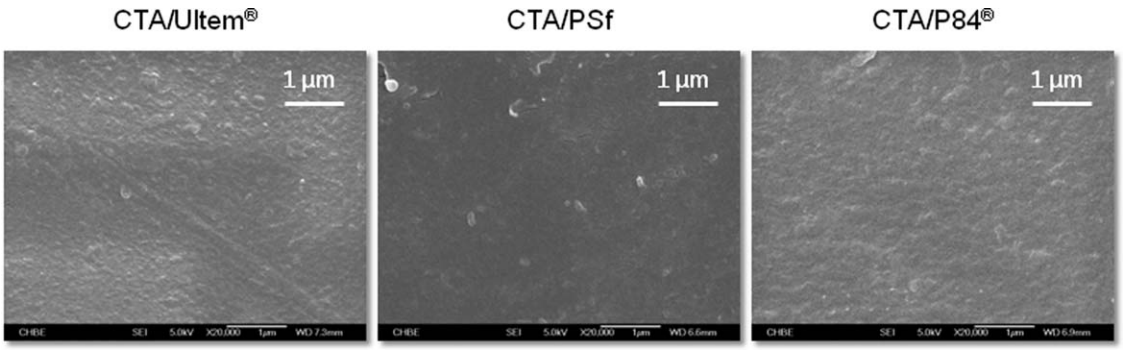

Figure 5. Top surface morphology of the fibers spun from various inner-layer materials.

Outer-layer dope flow rate: 0.1 mL/min; inner-layer dope flow rate: 1.5 mL/min; bore fluid flow rate: 1.0 mL/min.

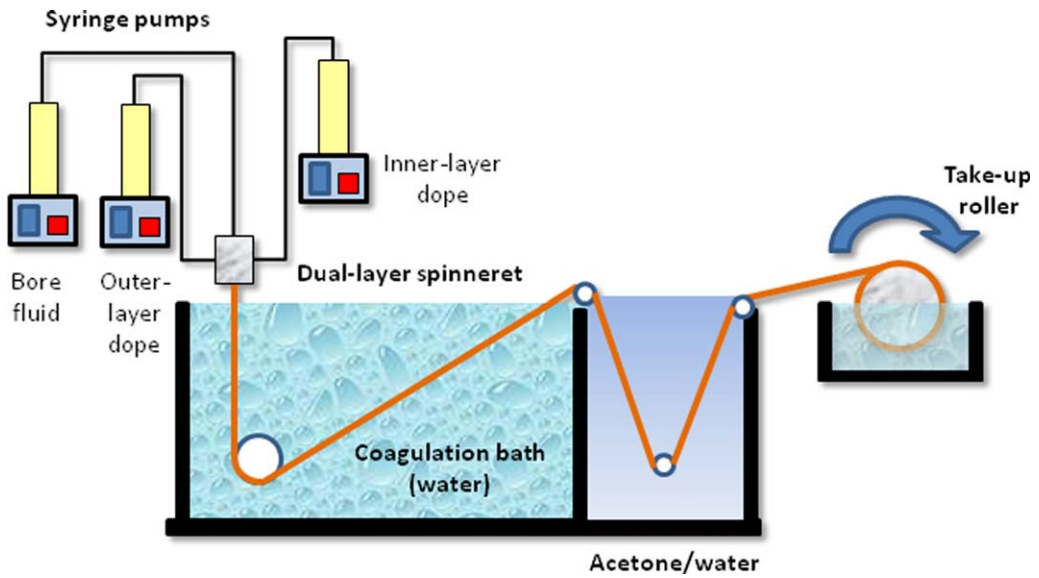

Figure 6. A dual-bath system of the spinning process.

[Color figure can be viewed in the online issue, which is available at wileyonlinelibrary.com.]

CTA can be partially dissolved/swelled by acetone while Ultem® is relatively inert for a short contact. The idea can be implemented by exposing the as-spun hollow fibers to acetone via a dual-bath spinning process as shown in Figure 6. A mixture of 85 wt % acetone and 15 wt % water is applied as the secondary external coagulant to provide a relative mild condition to create a defective top surface.

The top four rows of Table 4 show the effect of bore fluid flow rate on dehydration performance of ethanol. For both outer-layer dope flow rates of 0.2 and 0.4 mL/min, enhancements in separation factor are observed. The enhancement is much significant for the fibers spun with a small outer-layer dope flow rate of 0.2 mL/min. Figure 7 compares their morphology and indicates several factors possibly occurring as the bore fluid flow rate increases. First, there is a reduction in fiber wall thickness due to the increment of the lumen diameter.[62] In addition; a higher bore fluid facilitates a faster demixing so that a more porous inner skin may be formed.

Table 4. Performance of Hollow Fibers Spun with Various Spinning Parameters and Solvent Treatment

Membrane ID	Outer-layer flow rate (ml/min)	Bore fluid flow rate (ml/min)	Flux (kg/m^2h)	Water concentration in permeate (wt%)	Separation Factor (water/ethanol)
Bore fluid: 1.0 ml/min (BF1.0)					
CTA/Ultem®-A-BF1.0	0.2	1	2.64	85.3	30
CTA/Ultem®-B-BF1.0	0.4	1	1.49	95.6	116
Bore fluid: 1.2 ml/min (BF1.2)					
CTA/Ultem®-A-BF1.2	0.2	1.2	2.47	94.7	96
CTA/Ultem®-B-BF1.2	0.4	1.2	1.52	95.9	136
Solvent treated (T)					
T-CTA/Ultem®-A-BF1.2	0.2	1.2	2.57	95.4	120
T-CTA/Ultem®-B-BF1.2	0.4	1.2	1.69	95.4	124

Inner-layer dope flow rate: 1.5ml/min; air gap: 1.5 cm; take up speed: free fall
Solvent for treatment: Acetone/water (85/15 wt%)
Feed: Ethanol/water (85/15 wt%) at 50°C

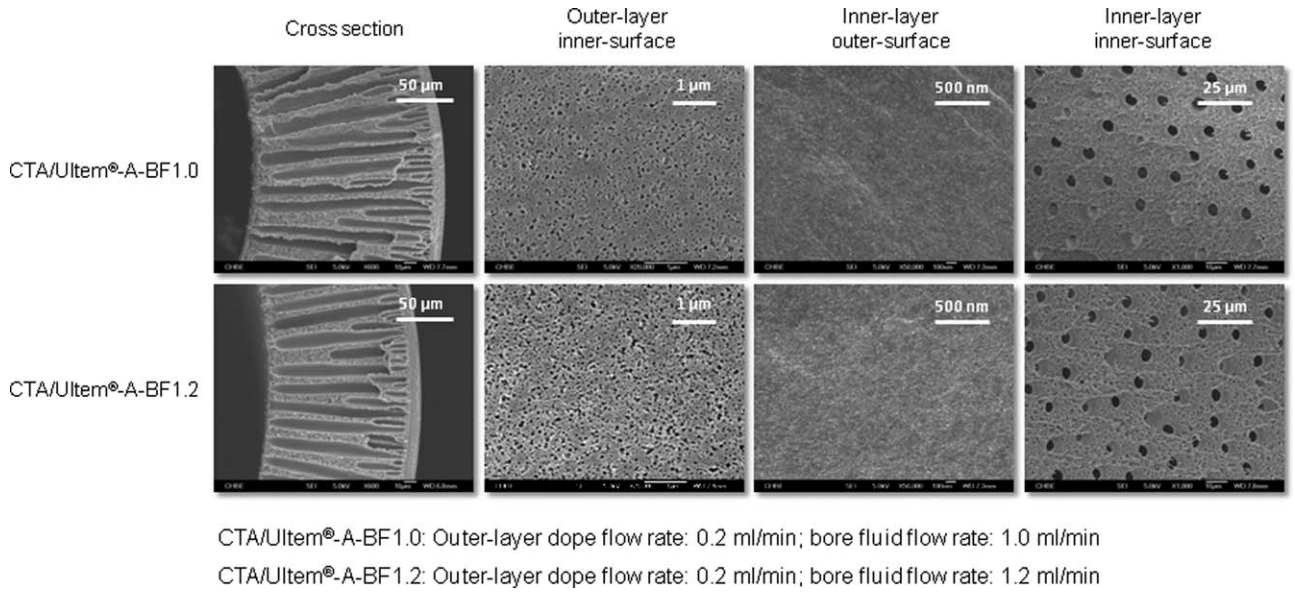

Figure 7. Morphology of the fibers spun from various bore fluid flow rates (without acetone treatment).

As a result, the transport resistance across the membrane is reduced and the flux is increased. Furthermore, a high bore fluid rate radially expands the nascent fiber. This may result in an increase in hoop elongation and induce molecular orientation along the circumference that enhances the separation factor.[62] On the other hand, the degrees of lumen expansion and hoop elongation are significantly reduced if a higher outer-layer dope flow rate of 0.4 mL/min is used because it is difficult to radially expand a nascent hollow fiber with a thick outer layer.

Positron annihilation spectroscopy (PAS) was used to probe the structure of the CTA outer layer as a function of positron energy/penetration depth. As depicted in Figure 8, a sharp reduction in R-parameter is observed around the positron energy of 1.5 keV which corresponds to the relatively dense structure at the outer surface.[27] Thereafter, the R-parameter starts to ascend and reaches a plateau, indicating transition from a relatively dense to a relatively porous structure. A comparison of the evolution profiles of R-parameter indicates that the fiber spun at the bore fluid flow rate of 1.0 mL/min has a fairly thick CTA skin layer as compared to the fiber spun at 1.2 mL/min due to hoop expansion and elongation as well as bore-fluid induced convective flow. Therefore, not only does the increase in bore fluid flow rate from 1.0 to 1.2 mL/min affect the dense selective layer in the Ultem® layer, but it also influences the cross-section morphology of the outer CTA layer.

The last two rows of Table 4 show the effect of acetone treatment on dehydration performance of ethanol. For the fiber spun at the outer-layer flow rate of 0.2 mL/min, the acetone treatment slightly improves the flux but considerably enhances the separation factor, while there is no much improvement on both flux and separation factor for the fiber spun at the outer-layer flow rate of 0.4 mL/min. For the former fiber, the acetone treatment may result in a more porous CTA outer skin and thus reduces the transport resistance. Based on the Huang-Feng model,[63] a reduction of substructure resistance can enhance both flux and separation factor for pervaporation membranes. As a result, the former fiber has a better flux and separation factor after the acetone treatment. Figure 9 compares the top skin morphology before and after the acetone treatment. It confirms our hypothesis that a more porous structure is formed after the acetone treatment. On the other hand, the acetone treatment has very limited effects on the fiber spun at the outer-layer flow rate of 0.4 mL/min because of a much thicker CTA layer.

Manipulation of the inner surface of the inner layer (i.e., inner surface)

In addition to the application of 95/5 wt % NMP/water as a bore fluid, two approaches are explored to study the effects of bore fluid chemistry on I^2PS fibers and to produce a fully

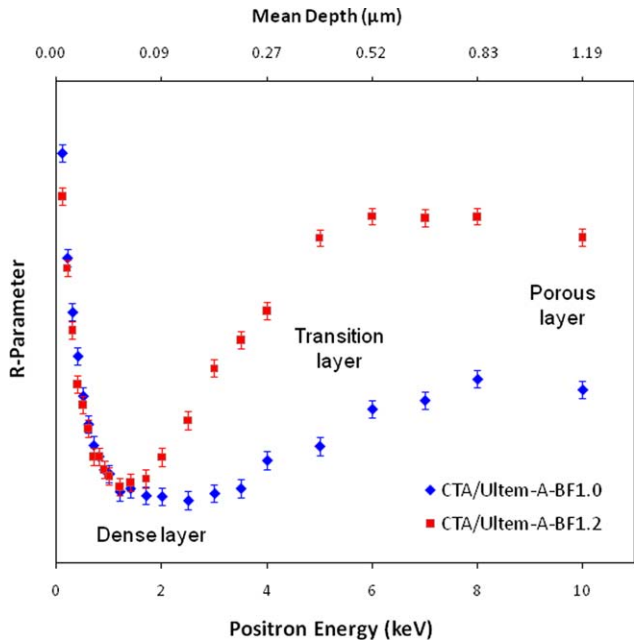

Figure 8. R-parameter vs. positron energy of the CTA/ Ultem® hollow fibers.

[Color figure can be viewed in the online issue, which is available at wileyonlinelibrary.com.]

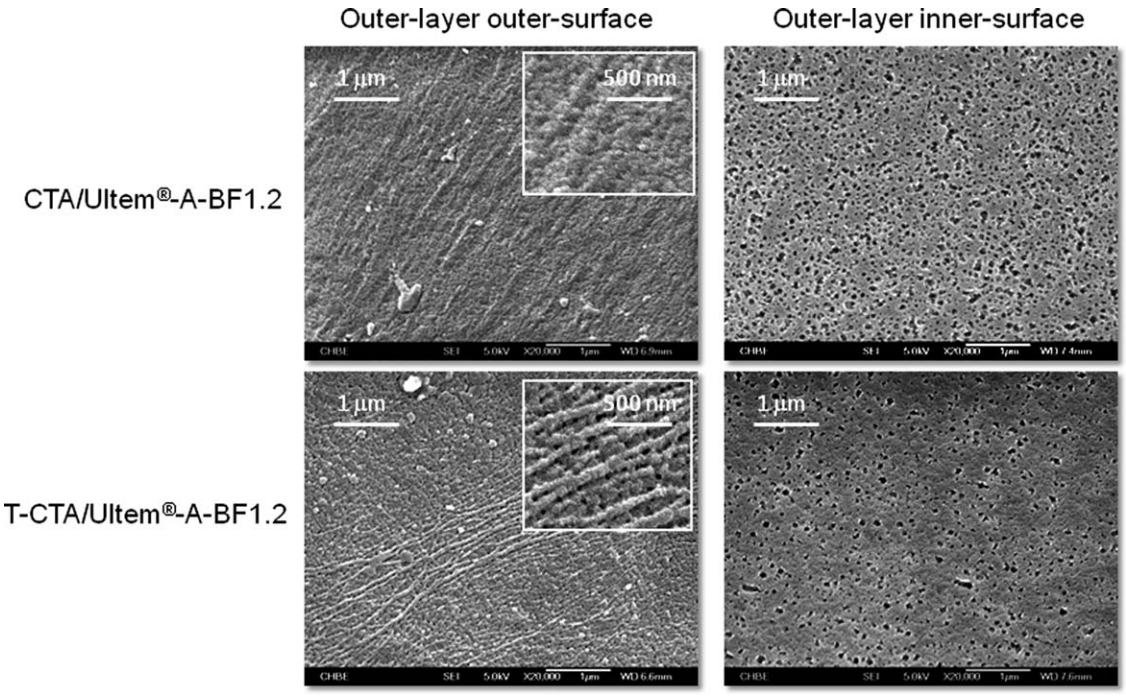

Figure 9. Surface morphology of the pristine (CTA/Ultem®-A-BF1.2), and acetone treated (T—CTA/Ultem®-A-BF1.2) fibers.

porous inner surface of the inner layer with a higher flux. They are (1) the usage of 95/5 wt % NMP/kerosene as a bore fluid, and (2) the combined employment of 10 wt % ethanol as a nonsolvent additive for the inner-layer dope solution and 95/5 wt % NMP/kerosene as a bore fluid. Figure 10 shows the inner surface and cross section morphology of the resultant fibers, while Table 5 compares their dehydration performance. There are drastic differences in the inner surface morphology. As shown in Table 2, kerosene has a much lower solubility parameter than other solvents and polymers, but it has a higher molecular weight than other solvents (i.e., water, NMP and ethanol). Furthermore, kerosene is miscible with ethanol but immiscible with water. Therefore, the incorporation of 5% kerosene into the NMP bore fluid may reduce the mass-transfer rate during phase inversion. Thus, mainly large pores are formed as shown in

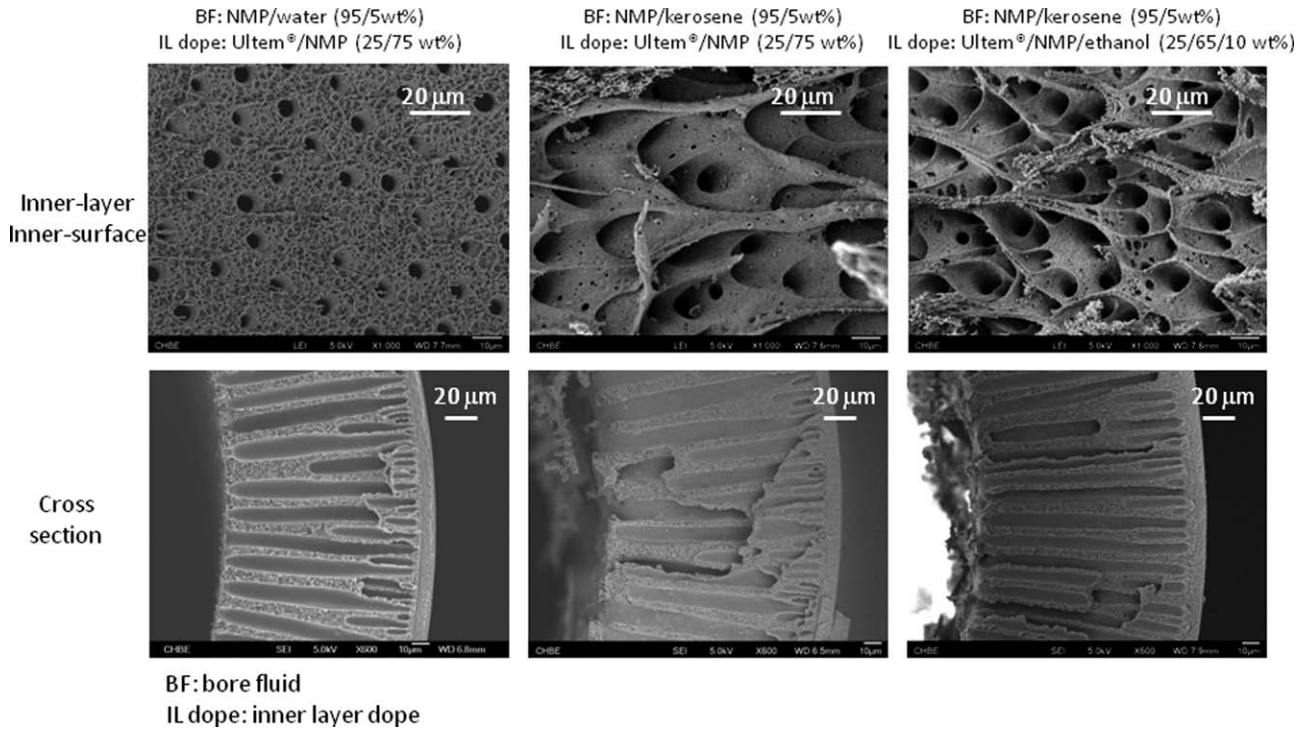

Figure 10. Inner-layer inner-surface and cross-section morphology of the hollow fiber spun with different bore fluids and inner layer dope solutions.

Table 5. Performance of Hollow Fibers Spun with Different Bore Fluid and Inner Layer Dope Compositions

Membrane ID	Inner-layer dope composition (wt%)	Bore fluid composition (wt%)	Flux (kg/m^{2}h)	Water concentration in permeate (wt%)	Separation Factor (water/ethanol)
CTA/Ultem®	Ultem®/NMP (25/75)	NMP/water (95/5)	2.47	94.7	96
CTA/Ultem®-K	Ultem®/NMP (25/75)	NMP/kerosene (95/5)	2.75	93.2	79
CTA/Ultem®-EK	Ultem®/NMP/ethanol (25/65/10)	NMP/kerosene (95/5)	3.04	91.8	62

CTA/Ultem®: NMP/water (95/5 wt%) as bore fluid
CTA/Ultem®-K : NMP/kerosene (95/5 wt%) as bore fluid
CTA/Ultem®-EK: Ultem®/NMP/ethanol (25/65/10 as inner-layer dope solution; NMP/kerosene (95/5 wt%) as bore fluid
Inner-layer dope flow rate: 1.5ml/min; Outer-layer dope flow rate: 0.2ml/min
Bore fluid flow rate 1.2 ml/min; air gap: 1.5 cm; take up speed: free fall
Feed: Ethanol/water (85/15 wt%) at 50°C

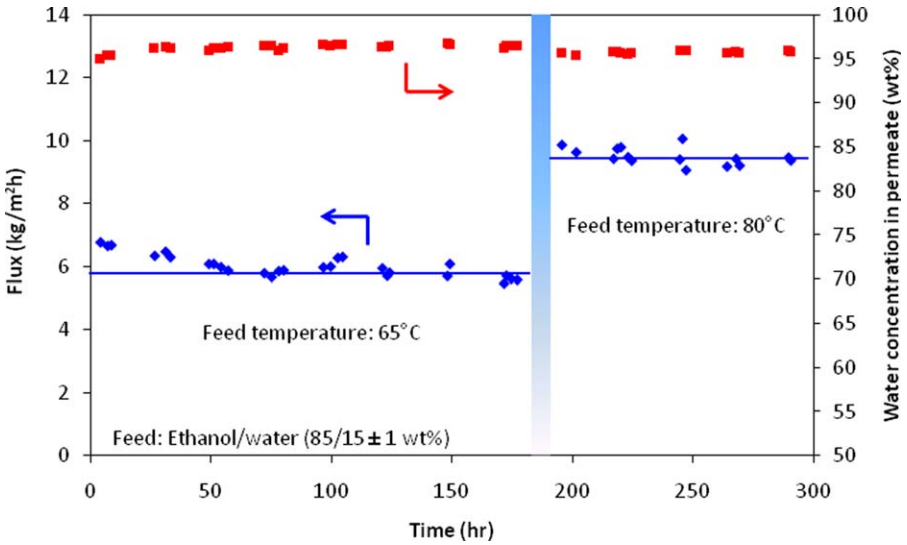

Figure 11. Stability of the hollow fiber (CTA/Ultem®-EK) in dehydration of ethanol.

[Color figure can be viewed in the online issue, which is available at wileyonlinelibrary.com.]

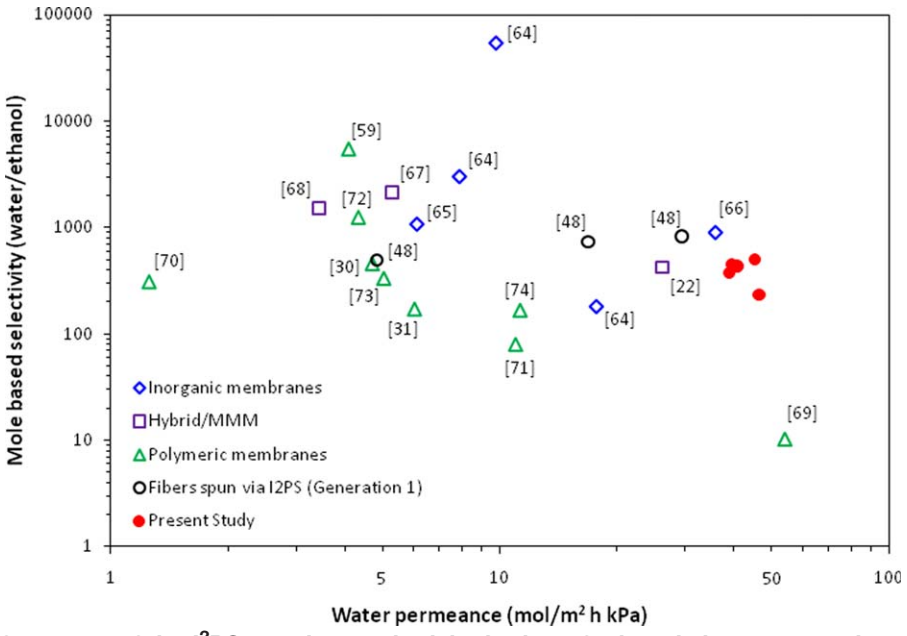

Figure 12. The performance of the I^{2}PS membranes in dehydration of ethanol via pervaporation.

For details see online Table S1 in supporting information. [Color figure can be viewed in the online issue, which is available at wileyonlinelibrary.com.]

Figure 10. On the other hand, the addition of a small amount of ethanol in the inner layer dope solution improves the mass transfer because kerosene and ethanol are miscible. As a result, a more porous surface structure is formed. In fact, the surface morphology of the fiber spun with the addition of ethanol in the inner layer dope solution possesses the most porous structure. As tabulated in Table 5, the hollow fiber spun with the ternary inner layer dope solution has the highest flux among all the investigated fibers with a minor sacrifice in separation factor.

Stability study and benchmarking

The stability of the hollow fiber spun with the ternary inner-layer dope solution was evaluated for 300 h. The permeate side of the fiber was maintained around 7–15 mbar using a two-stage diaphragm pump during the idle mode with a continuous circulation of feed solution. Thereafter, the vacuum was lowered to 1 mbar for the sample collection using a rotary pump. The performance of the fiber was initially monitored at 65°C for around 200 h. Subsequently, the temperature of the feed solution was raised to 80°C to verify the stability of the same fiber at a higher operating temperature. Figure 11 depicts the performance stability of the hollow fiber (CTA/Ultem®-EK) as functions of time and feed temperature. The fiber possesses a relatively stable performance throughout the monitored period. After 180 h at 65°C, the flux stabilizes at about 5.8 kg/m^2 h with a permeate water purity of 96.2 wt %. The flux is further increased to 9.5 kg/m^2 h with a permeate water purity of 95.8 wt % when the feed temperature is raised to 80°C. For benchmarking, Figure 12 compares the newly developed second generation I^{2}PS membranes with literatures in terms of mole-based selectivity and permeance (details of the figure are shown online in Table S1 in supporting information). All hollow fibers spun via I^{2}PS possess a relatively high permeance and reasonable selectivity as compared to other membranes, signifying the feasibility of using these I^{2}PS hollow fibers for dehydration of ethanol via pervaporation.

Conclusions

We have conducted a fundamental study on the immiscible induced phase separation (I^{2}PS) process and explored the science and engineering to design hollow fibers with high permeance and selectivity for pervaporation. It has been found that membranes with a highly porous inner surface of the outer layer can be developed by co-spinning of relatively incompatible materials such as cellulose triacetate (CTA) and polysulfone (PSf) as the outer and inner layer materials, respectively. Fibers with much loose or high outer surface porosity can be designed by a short immersion in acetone during spinning to partially dissolve the outer CTA protective layer. Interestingly, by simultaneously incorporating a small amount of kerosene as a nonsolvent into the bore fluid and a small amount of ethanol into the inner-layer dope solution, the permeation flux of the resultant fiber are improved. The following conclusions can, therefore, be drawn:

- The selection of inner layer materials has significant effects on the inner surface morphology of the outer layer. A relatively incompatible inner and outer layer tends to produce dual-layer hollow fibers with a highly porous inner surface of the outer layer.
- The delamination between inner and outer layers must be prevented in order to take the advantages of the shielding effect from the outer protective layer and to minimize inner layer swelling. Since the water/ethanol selectivity of the acetone treated fiber is comparable to the pristine fiber, the selectivity of the fiber is mainly controlled by the inner-layer outer-surface.
- The dual-layer fiber spun from the I^{2}PS process shows a stable performance throughout the monitored period of 300 h (200 h at 65°C followed by 100 h at 80°C) signifying its feasibility in dehydration of ethanol via pervaporation process. The flux reaches 9.5 kg/m^2 h with a permeate water purity of 95.8 wt % when the feed temperature is 80°C.

Acknowledgments

The authors would like to acknowledge the financial support provided by National Research Foundation of Singapore (NRF) under its Competitive Research Program for the project entitled, "New Biotechnology for Processing Metropolitan Organic Wastes into Value-Added Products" (grant number: R-279-000-311-281), Eastman Chemical Co. (USA) for providing CTA polymer. Special thanks are dedicated to Dr. Natalia Widjojo, Dr. Panu Sukitpaneenit, and Ms. Felinia Edwie for providing valuable assistances and suggestions to this research.

Notation

A = effective area of membrane, m^2
E_+ = incident positron energy, keV
$f_{i,f}$ = fugacity of component i in feed, kPa
$f_{i,p}$ = fugacity of component i in permeate, kPa
J = flux of the membrane, kg m^{-1} h^{-1}
$\frac{P}{l}$ = permeance, mol m^{-2} kPa^{-1} h^{-1}
p_i^{sat} = saturated vapor pressure of component i, kPa
Q = total weight of permeate collected at time interval, kg
x_i = mass fraction of component i
x_w = mass fraction of water at feed
y_w = mass fraction of water at permeate
Z = average implantation depth of positronium, nm

Greek letters symbols

α = selectivity of the membrane, mole water/mol ethanol
γ_i = activity coefficient of component i
ρ = density of the polymer material, g/cm^3

Literature Cited

1. Kober PA. Pervaporation, perstillation and percrystallization. *J Am Chem Soc*. 1917;39:944–948.
2. Binning RC, Lee RJ, Jennings JF, Martin EC. Separation of liquid mixtures by permeation. *Ind Eng Chem*. 1961;53:45–50.
3. Chiang R, Perry E. *Process for separating aqueous formaldehyde mixtures*. US Patent 4067805, 1976.
4. Perry E. *Membrane separation of organics from aqueous solutions*. US Patent 4218312, 1980.
5. Aptel P, Challard N, Cuny J, Neel J. Application of the pervaporation process to separate azeotropic mixtures. *J Membr Sci*. 1976;1: 271–287.
6. Neel J, Nguyen QT, Clement R, Le Blanc L. Fractionation of a binary liquid mixture by continuous pervaporation. *J Membr Sci*. 1983;15:43–62.
7. Feng X, Huang RYM. Liquid separation by membrane pervaporation: a review. *Ind Eng Chem Res*. 1997;36:1048–1066.
8. Shao P, Huang RYM. Polymeric membrane pervaporation. *J Membr Sci*. 2007;287:162–179.
9. Chapman PD, Oliveira T, Livingston AG, Li K. Membranes for the dehydration of solvents by pervaporation. *J Membr Sci*. 2008;318:5–37.
10. Vane LM. A review of pervaporation for product recovery from biomass fermentation processes. *J Chem Technol Biotechnol*. 2005;80: 603–629.

11. Vane LM. Separation technologies for the recovery and dehydration of alcohols from fermentation broths. *Biofuels Bioprod Biorefin.* 2008;2:553–588.
12. Huang Y, Baker RW, Vane LM. Low-energy distillation-membrane separation process. *Ind Eng Chem Res.* 2010;49:3760–3768.
13. Huang Y, Ly J, Nguyen D, Baker RW. Ethanol dehydration using hydrophobic and hydrophilic polymer membranes. *Ind Eng Chem Res.* 2010;49:12067–12073.
14. Jiang LY, Wang Y, Chung TS, Qiao XY, Lai JY. Polyimides membranes for pervaporation and biofuels separation. *Prog Poly Sci.* 2009;34:1135–1160.
15. Peng M, Vane LM, Liu SX. Recent advances in VOCs removal from water by pervaporation. *J Hazard Mater.* 2003;98:69–90.
16. Fouad EA, Feng X. Pervaporative separation of n-butanol from dilute aqueous solutions using silicalite-filled poly(dimethyl siloxane) membranes. *J Membr Sci.* 2009;339:120–125.
17. Smitha B, Suhanya D, Sridhar S, Ramakrishna, M. Separation of organic-organic mixtures by pervaporation – a review. *J Membr Sci.* 2004;241:1–21.
18. Ong YK, Widjojo N, Chung TS. Fundamentals of semi-crystalline poly(vinylidene fluoride) membrane formation and its prospects for biofuel (ethanol and acetone) separation via pervaporation. *J Membr Sci.* 2011;378:149–162.
19. Tusel GF, Brüschke HEA. Use of pervaporation systems in the chemical industry, *Desalination.* 1985;53:327–338.
20. Brüschke H. *Multi-layer membrane and the use thereof for the separation of liquid mixtures according to the pervaporation process.* US Patent 4755299, 1985.
21. Morigami Y, Kondo M, Abe J, Kita H, Okamoto K. The first large-scale pervaporation plant using tubular-type module with zeolite NaA membrane. *Sep Purif Technol.* 2001;25:251–260.
22. Kreiter R, Rietkerk MDA, Castricum HL, van Veen HM, ten Elshof JE, Vente JF. Stable hybrid silica nanosieve membranes for the dehydration of lower alcohols. *ChemSusChem.* 2009;2:158–160.
23. Peng N, Widjojo N, Sukitpaneenit P, Teoh MM, Lipscomb GG, Chung TS, Lai JY. Evolution of polymeric hollow fibers as sustainable technologies: past, present, and future. *Prog Poly Sci.* 2012;37:1401–1424.
24. Li DF, Chung TS, Wang R, Liu Y. Fabrication of fluoropolyimide/polyethersulfone (PES) dual-layer asymmetric hollow fiber membranes for gas separation. *J Membr Sci.* 2002;198:211–223.
25. Henne W, Dünweg G, Schmitz W, Pohle R, Lawitzki F. *Dialyzing membrane with adsorbent layer*, US Patent 4267047, 1981.
26. Hosseini SS, Peng N, Chung TS. Gas separation membranes developed through integration of polymer blending and dual-layer hollow fiber spinning process for hydrogen and natural gas enrichments. *J Membr Sci.* 2010;349:156–166.
27. Li FY, Li Y, Chung TS, Chen H, Jean YC, Kawi S. Development and positron annihilation spectroscopy (PAS) characterization of polyamide imide (PAI) polyethersulfone (PES) based defect-free dual-layer hollow fiber membranes with an ultrathin dense-selective layer for gas separation. *J Membr Sci.* 2011;378:541–550.
28. Sun SP, Wang KY, Peng N, Hatton TA, Chung TS. Novel polyamide imide/cellulose acetate dual-layer hollow fiber membranes for nanofiltration. *J Membr Sci.* 2010;363:232–242.
29. Edwie F, Teoh MM, Chung TS. Effects of additives on dual-layer hydrophobic-hydrophilic PVDF hollow fiber membranes for membrane distillation and continuous performance. *Chem Eng Sci.* 2012;68:567–578.
30. Widjojo N, Chung TS. Pervaporation dehydration of C2-C4 alcohols by 6FDA-ODA-NDA/Ultem® dual-layer hollow fiber membranes with enhanced separation performance and swelling resistance. *Chem Eng J.* 2009;155:736–743.
31. Wang Y, Goh SH, Chung TS, Na P. Polyamide-imide/polyetherimide dual-layer hollow fiber membranes for pervaporation dehydration of C1-C4 alcohols. *J Membr Sci.* 2009;326:222–233.
32. Li DF, Chung TS, Wang R. Morphological aspects and structure control of dual-layer asymmetric hollow fiber membranes formed by a simultaneous co-extrusion approach. *J Membr Sci.* 2004;243:155–175.
33. Widjojo N, Chung TS, Krantz WB. A morphological and structural study of Ultem/P84 copolyimide dual-layer hollow fiber membranes with delamination-free morphology. *J Membr Sci.* 2007;294:132–146.
34. Jiang LY, Chung TS, Cao C, Huang Z, Kulprathipanja S. Fundamental understanding of nano sized zeolite distribution in the formation of the mixed matrix single- and dual-layer asymmetric hollow fiber membranes. *J Membr Sci.* 2005;252:89–100.
35. Li Y, Chung TS, Huang Z, Kulprathipanja S. Dual-layer polyethersulfone (PES)/BTDA TDI/MDI co-polyimide (P84) hollow fiber membranes with a submicron PES-zeolite beta mixed matrix dense-selective layer for gas separation. *J Membr Sci.* 2006;277:28–37.
36. Sukitpaneenit P, Chung TS, PVDF/nanosilica dual-layer hollow fibers with enhanced selectivity and flux as novel membranes for ethanol recovery. *Ind Eng Chem Res.* 2012;51:978–993.
37. Yang TX, Shi GM, Chung TS. Symmetric and asymmetric zeolitic imidazolate frameworks (ZIFs)/polybenzimidazole (PBI) nanocomposite membranes for hydrogen purification at high temperatures. *Adv Energy Mater.* 2012;2:1358–1367.
38. Husain S, Koros WJ. Mixed matrix hollow fiber membranes made with modified HSSZ-13 zeolite in polyetherimide polymer matrix for gas separation. *J Membr Sci.* 2007;288:195–207.
39. He T, Mulder MHV, Wessling M. Preparation of porous hollow fiber membranes with a triple-orifice spinneret. *J Appl Polym Sci.* 2003;87:2151–2157.
40. Bonyadi S, Chung TS. Highly porous and macrovoid-free PVDF hollow fiber membranes for membrane distillation by a solvent-dope solution co-extrusion approach. *J Membr Sci.* 2009;331:66–74.
41. Wang P, Teoh MM, Chung TS. Morphological architecture of dual-layer hollow fiber for membrane distillation with higher desalination performance. *Water Res.* 2011;45:5489–5500.
42. Jiang LY, Chen H, Jean YC, Chung TS. Ultrathin polymeric interpenetration network with separation performance approaching ceramic membranes for biofuel. *AIChE J.* 2009;55:75–86.
43. Kopeć KK, Dutczak SM, Wessling M, Stamatialis DF. Chemistry in a spinneret-On the interplay of crosslinking and phase inversion during spinning of novel hollow fiber membranes. *J Membr Sci.* 2011;369:308–318.
44. Henis JMS, Tripodi MK. Multicomponent Membrane for Gas Separations. US Patent 4230463, 1980.
45. Makino H, Kusuki Y, Harada T, Shimazaki H, Isida T. Aromatic Polyimide Composite Separating Membrane. US Patent 4528004, 1985.
46. Bikson B, Nelson JK. Production and use of Improved Composite Fluid Separation Membranes. US Patent 5356459, 1994.
47. Huang Y, Baker RW, Aldajani T, Ly J. Dehydration Processes using Membranes with Hydrophobic Coating. WIPO Patent Application WO/2009/029719, 2009.
48. Ong YK, Chung TS. High performance dual-layer hollow fiber fabricated via novel immiscibility induced phase separation (I^2PS) process for dehydration of ethanol. *J Membr Sci.* 2012;421-422:271–282.
49. Zhang S, Wang KY, Chung TS, Jean YC, Chen H. Molecular design of the cellulose ester-based forward osmosis membranes for desalination. *Chem Eng Sci.* 2011;66:2008–2018.
50. Chen H, Hung WS, Lo CH, Huang SH, Cheng ML, Liu G, Lee KR, Lai JY, Sun YM, Hu CC, Suzuki R, Ohdaira T, Oshima N, Jean YC. Free-volume depth profile of polymeric membranes studied by positron annihilation spectroscopy: layer structure from interfacial polymerization. *Macromol.* 2007;40:7542–7557.
51. Jean YC, Hung WS, Lo CH, Chen H, Liu G, Chakka L, Cheng ML, Nanda D, Tung KL, Huang SH, Lee KR, Lai JY, Sun YM, Hu CC, Yu CC. Applications of positron annihilation spectroscopy to polymeric membranes. *Desalination.* 2008;234:89–98.
52. Baker RW, Wijmans JG, Huang Y. Permeability, permeance and selectivity: A preferred way of reporting pervaporation performance data. *J Membr Sci.* 2010;348:346–352.
53. Qiao X, Chung TS. Fundamental characteristics of sorption, swelling, and permeation of P84 co-polyimide membranes for pervaporation dehydration of alcohols. *Ind Eng Chem Res.* 2005;44:8938–8943.
54. Ong RC, Chung TS. Fabrication and positron annihilation spectroscopy (PAS) characterization of cellulose triacetate membranes for forward osmosis. *J Membr Sci.* 2012;394–395:230–240.
55. Scheirs J. *A Guide to Polymeric Geomembranes: A Practical Approach.* Chichester UK: John Wiley & Sons, Ltd., 2009.
56. Peng N, Chung, TS, Wang KY. Macrovoid evolution and critical factors to form macrovoid free hollow fiber membranes. *J Membr Sci.* 2008;318:363–372.
57. Vogrin N, Stropnik C, Musil V, Brumen M. The wet phase separation: the effect of cast solution thickness on the appearance of macrovoids in the membrane forming ternary cellulose acetate/acetone/water system. *J Membr Sci.* 2002;207:139–141.
58. Li DF, Chung TS, Ren JZ, Wang R. Thickness dependence of macrovoid evolution in wet phase-inversion asymmetric membranes. *Ind Eng Chem Res.* 2004;43:1553–1556.

59. Qiao X, Chung TS, Pramoda KP. Fabrication and characterization of BTDA-TDI/MDI (P84) co-polyimide membranes for the pervaporation dehydration of isopropanol. *J Membr Sci*. 2005;264:176–189.
60. Liu RX, Qiao XY, Chung TS. The development of high performance P84 co-polyimide hollow fibers for pervaporation dehydration of isopropanol. *Chem Eng Sci*. 2005;60:6674–6686.
61. Jiang LY, Song ZW. Interfacial resistance of dual-layer asymmetric hollow fiber pervaporation membranes formed by co-extrusion. *J. Polym. Res*. 2011;18:2505–2514.
62. Wang Y, Gruender M, Chung TS. Pervaporation dehydration of ethylene glycol through polybenzimidazole (PBI)-based membranes. 1. Membrane fabrication. *J Membr Sci*. 2010;363:149–159.
63. Huang RYM, Feng X. Resistance model approach to asymmetric polyetherimide membranes for pervaporation of isopropanol/water mixtures. *J Membr Sci*. 1993;84:15–27.
64. Sommer S, Melin T. Performance evaluation of microporous inorganic membranes in the dehydration of industrial solvents. *Chem Eng Process*. 2005;44:1138–1156.
65. Tanaka K, Yoshikawa R, Ying C, Kita H, Okamoto KI. Application of zeolite membranes to esterification reactions. *Catal Today* 2011; 67:121–125.
66. Zhou H, Korelskiy D, Leppäjärvi T, Grahn M, Tanskanen J, Hedlund J. Ultrathin zeolite X membranes for pervaporation dehydration of ethanol. *J Membr Sci*. 2012;399-400:106–111.
67. Huang Z, Shi Y, Wen R, Guo YH, Su JF. Matsuura T. Multilayer poly-(vinyl alcohol)-zeolite 4A composite membranes for ethanol dehydration by means of pervaporation. *Sep Purif Technol*. 2006;51:126–136.
68. Qiu S, Wu L, Shi G, Zhang L, Chen H, Gao C. Preparation and pervaporation property of chitosan membrane with functionalized multiwalled carbon nanotubes. *Ind Eng Chem Res*. 2010;49:11667–11675.
69. Chen Y, Xiangli F, Jin W, Xu N. Organic-inorganic composite pervaporation membranes prepared by self-assembly of polyelectrolyte multilayers on macroporous ceramic supports. *J Membr Sci*. 2007;302:78–86.
70. Van Baelen D, Van der Bruggen B, Van den Dungen K, Degreve J, Vandecasteele C. Pervaporation of water-alcohol mixtures and acetic acid-water mixtures. *Chem Eng Sci*. 2005;60:1583–1590.
71. Tsai HA, Hong MJ, Huang GS, Wang YC, Li CL, Lee KR, Lai JY. Effect of DGDE additive on the morphology and pervaporation performances of asymmetric PSf hollow fiber membranes. *J Membr Sci*. 2002;208:233–245.
72. Huang RYM, Pal R, Moon GY. Pervaporation dehydration of aqueous ethanol and isopropanol mixtures through alginate/chitosan two ply composite membranes supported by poly(vinylidene fluoride) porous membrane. *J Membr Sci*. 2000;167:275–289.
73. Ong YK, Wang H, Chung TS. A prospective study on the application of thermally rearranged acetate-containing polyimide membranes in dehydration of biofuels via pervaporation. *Chem Eng Sci*. 2012;79:41–53.
74. Chen J, Chen X, Yin X, Ma J, Jiang Z. Bioinspired fabrication of composite pervaporation membranes with high permeation flux and structural stability. *J Membr Sci*. 2009;344:136–143.

Manuscript received Dec. 6, 2012, and revision received Mar. 15, 2013.